Numerical Solution of the Constrained Wigner Equation

Robert Kosik, Johann Cervenka, and Hans Kosina
Institute for Microelectronics, TU Wien, Vienna, Austria
http://www.iue.tuwien.ac.at
{kosik,cervenka,kosina}@iue.tuwien.ac.at

***Abstract*—Quantum electron transport in modern semiconductor devices can be described by a Wigner equation which is formally similar to the classical Liouville equation. The stationary Wigner equation has a singularity at zero momentum (k=0). In order to get a non-singular solution it is necessary to impose a constraint for the solution at k=0 which gives the constrained Wigner equation. We introduce a Petrov-Galerkin method for the solution of the corresponding constrained sigma equation. The constraint in the Wigner equation is interpreted as an extra test function and is naturally incorporated in the method.**

***Index Terms*—Wigner function, sigma function, constrained equation, quantum transport, device simulation, resonant tunneling diode, Galerkin method**

I. Introduction

The Wigner function method [1] is based on a mathematical formulation of quantum mechanics which is close to a classical phase space description [2], [3]. This allows for flexible mixed quantum-classical models and makes it an attractive approach for many applications where only parts of the system need to be modeled fully quantum mechanically [4].

Quantum electron transport in modern semiconductor devices can be described by a Wigner equation which is formally similar to the classical Liouville equation (also called Vlasov equation). The existence and uniqueness of solutions to the stationary Wigner equation with classical inflow boundary conditions is a long-standing open problem even in a single spatial dimension [5], [6].

Solution methods for the Wigner equation can be divided into deterministic and stochastic methods. Much of the practical work using the Wigner equation is based on Monte Carlo methods [7]. In the classical case, Monte Carlo methods are more versatile than deterministic methods. In particular, they can solve the Vlasov equation with inflow boundary conditions.

In previous work [8] we have argued that the constrained Wigner equation is a viable option for a deterministic solution of the stationary Wigner equation which is well-behaved at $k=0$. Below we introduce a deterministic numerical method for the solution of the constrained Wigner equation.

This work was partly funded by FWF Austrian Science Fund, project number P33151 "Numerical Constraints for the Wigner and the Sigma Equation".

II. Sigma and Wigner Function

Stationary quantum transport is described by the Liouville-von Neumann equation for the density matrix $\rho(x,y)$

$$-\tfrac{\hbar^2}{2m}\left(\tfrac{\partial^2}{\partial x^2}-\tfrac{\partial^2}{\partial y^2}\right)\rho+\big(V(x)-V(y)\big)\rho=0 \qquad (1)$$

where $V(x)$ is the potential energy.

From the density matrix $\rho(x,y)$ the Wigner function $f(r,k)$ is defined as the result of two consecutive transformations:

1) Introduce new coordinates for the quantum density

$$r=\frac{x+y}{2}, \qquad s=x-y.$$

Using these coordinates the density matrix transforms into the sigma function

$$\sigma(r,s)=\rho(r+\frac{s}{2},r-\frac{s}{2}). \qquad (2)$$

2) The Wigner function $f(r,k)$ is derived from the sigma function $\sigma(r,s)$ via a Fourier transform in coordinate s

$$f(r,k)=\frac{1}{2\pi}\int\sigma(r,s)\,e^{-i\,k\,s}\,ds. \qquad (3)$$

The sigma function has the symmetry property

$$\sigma(r,s)=\overline{\sigma(r,-s)}=a(r,s)+ib(r,s). \qquad (4)$$

The real part $a(r,s)$ is an even function, the imaginary part $b(r,s)$ is an odd function of variable s.

III. Sigma and Wigner Equation

Using coordinates (r,s) the stationary von Neumann equation transforms into the stationary sigma equation

$$\frac{\hbar^2}{m}\frac{\partial^2\sigma}{\partial r s}=U(r,s)\sigma(r,s) \qquad (5)$$

where the potential term $U(r,s)$ is defined by

$$U(r,s)=V\left(r+\frac{s}{2}\right)-V\left(r-\frac{s}{2}\right). \qquad (6)$$

Applying the Fourier transform (3) to the sigma equation (5) gives the stationary Wigner equation

$$\frac{\hbar k}{m}\frac{\partial f(r,k)}{\partial r}=\int f(r,k-k')V_w(r,k')dk'. \qquad (7)$$

Here the Wigner potential $V_w(r,k)$ is defined as the Fourier transform of $U(r,s)$ divided by $i\hbar$

$$V_w(r,k) = \frac{1}{i\hbar}\frac{1}{2\pi}\int U(r,s)\, e^{-i\,k\,s}\, ds. \tag{8}$$

Classical inflow boundary conditions are imposed on the stationary Wigner equation at the spatial boundaries $r_{\min}$, $r_{\max}$.

IV. Constrained Wigner and Sigma Equation

In a single spatial dimension the Wigner equation (7) can be rewritten for $k \neq 0$ as

$$\frac{\partial f(r,k)}{\partial r} = \frac{1}{k}\frac{m}{\hbar}\int f(r,k-k')V_w(r,k')dk'. \tag{9}$$

The form (9) emphasizes that the equation becomes singular at $k=0$. In order to avoid the singularity one has to impose two equations for $k=0$

1) Putting $k=0$ in (7) gives the following integrability constraint [5], [6]

$$\int f(r,k')V_w(r,-k')dk' = 0. \tag{10}$$

2) In the limit $k \to 0$ equation (9) reduces to the "transport" equation at $k=0$

$$\frac{\partial f(r,0)}{\partial r} = \frac{m}{\hbar}\int f_k(r,-k')V_w(r,k')dk'. \tag{11}$$

Together these equations define an overdetermined system which we call the constrained Wigner equation.

By inverse Fourier transform a corresponding constrained sigma equation can be derived [8] which consists in equation (5) plus double homogeneous boundary conditions

$$\sigma(r,s_{\max}) = \sigma(r,-s_{\max}) = 0. \tag{12}$$

With double homogeneous boundary conditions the sigma equation is overdetermined as well.

V. Spectral Method

In previous work [8] we solved the constrained sigma equation directly in a least squares sense using finite differences. Here we solve the constrained sigma equation by a spectral approach with sine and cosine ansatz functions. This ansatz amounts to a solution in the Fourier domain, i.e., a solution of the constrained Wigner equation. Improving on [8] we also incorporate a complex absorbing potential

$$\tilde{U}(r,s) = U(r,s) + iW(s) \tag{13}$$

in order to diminish unphysical reflections of outgoing waves as advocated in [9].

For the numerical solution we first discretize the sigma equation (5) in coordinate r using finite differences

$$\frac{\hbar^2}{m}\frac{\sigma_s(r_{i+1},s)-\sigma_s(r_i,s)}{\triangle r} = \frac{\tilde{U}(r_i,s)\sigma(r_i,s)+\tilde{U}(r_{i+1},s)\sigma(r_{i+1},s)}{2}. \tag{14}$$

The semi-discrete equation (14) is then discretized in coordinate s by employing a Petrov-Galerkin approach where the set of ansatz functions is different from the set of test functions. The ansatz functions for a, b from (4) fulfill the homogeneous boundary conditions (12)

$$a(r_i,s) = \sum_{n=1}^{N_k} a_n(r_i)\cos\left(\frac{2n-1}{2}\triangle k s\right) \tag{15}$$

$$b(r_i,s) = \sum_{n=1}^{N_k} b_n(r_i)\sin\left(n\triangle k s\right). \tag{16}$$

Our test functions are the union of two families

$$T_n^a = \sin\left(\frac{2n-1}{2}\triangle k s\right)\ (n=1\ldots N_k) \tag{17}$$

$$T_n^b = \cos(n\triangle k s) \qquad (n=0\ldots N_k) \tag{18}$$

which were chosen because they are the derivatives $\frac{\partial}{\partial_s}$ of the ansatz functions. With this we have $2N_k$ ansatz functions and $2N_k+1$ test functions. The test function $T_0^b = 1$ is extra and the corresponding equations represent the integrability constraint. Inflow boundary conditions and an equation enforcing exact conservation of mass are imposed as constraints.

VI. Implementation

The overdetermined system is solved in a least squares sense with constraints exactly fulfilled. Mathematically this represents a quadratic programming problem with linear equality constraints. For the solution we introduce the error vector e

$$e = Ax - b \tag{19}$$

where matrix A and vector b represent the system matrix and right hand side from the Petrov-Galerkin equations. (In our case the right hand side b is zero.) The vector x represents the unknown coefficients of the ansatz functions.

In order to find the constrained least squares solution we minimize $\|e\|^2$ using the method of Lagrange multipliers. The equations (19) are interpreted as the definition of e and are imposed as constraints (introducing one Lagrange multiplier for each equation). We also add the constraints for the boundary conditions and for the exact discrete conservation of mass. This method gives a linear system in variables x and e plus the Lagrange multipliers λ. The resulting system has an increased number of unknowns but avoids building the normal equations. This is a trade-off between numerical accuracy (condition number) and system size.

To deal with high memory requirements a specialized solver for the solution of the banded linear system is deployed.

VII. Numerical Evaluation

The spectral method is evaluated by simulating a GaAs/AlGaAs resonant tunneling diode (RTD) and comparison with the quantum transmitting boundary method (QTBM) which we take as the reference model.

The RTD model used in the simulation is depicted in Fig. 1, which consists of a $4.5\,\mathrm{nm}$-wide GaAs quantum well and $2.8\,\mathrm{nm}$-wide AlGaAs barrier layers. Doped GaAs electrode layers of $30\,\mathrm{nm}$ are included on each side of the device. The potential drops linear between barriers. Outside the

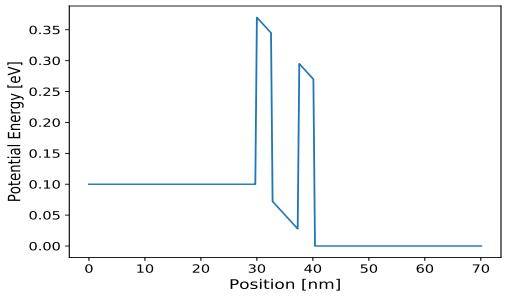

Fig. 1: Structure of the resonant tunneling diode with two AlGaAs barrier layers as used in the simulation. In the plotted example a bias of -0.1 V is assumed.

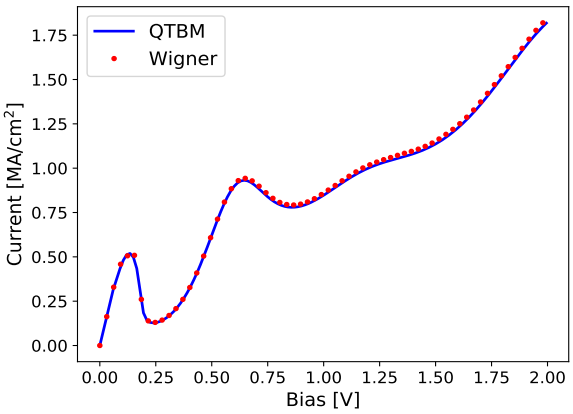

Fig. 2: Simulation of a resonant tunneling diode and comparison with QTBM. A weak second resonance near 0.7 V is shown.

electrodes, reservoirs characterized by the thermal equilibrium distributions of carriers are assumed. The conduction band discontinuity is taken to be 0.27 eV.

We demonstrate the numerical capability of the method in Fig. 2 by simulating up to a high bias which is beyond the usual operating conditions of the device. The QTBM and the Wigner function model fit almost perfectly up to a bias of 2 V. In Fig. 3 we plot the particle density in the active region of the device for varying biases. Again, the fit between QTBM and Wigner is reasonably good.

In order to achieve high accuracy, a coherence length of at least 60 nm must be assumed and a fine mesh with $N_r \sim 800$ points has to be used for the simulation. Consequently, numerical costs are high as the Wigner equation is dense in variable k and the incorporation of constraints complicates the solution.

VIII. Conclusion

Using a large coherence length and a sufficiently fine mesh the constrained Wigner equation reproduces results from the QTBM reliably and with good accuracy.

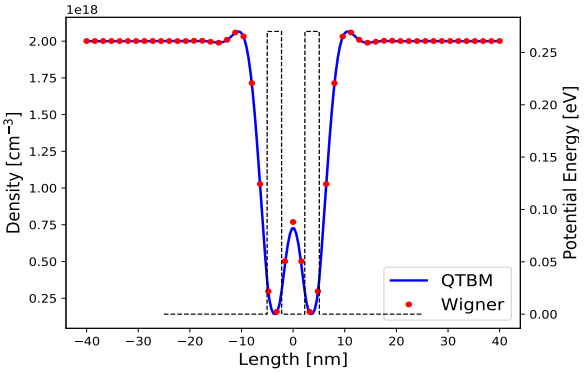

(a) Bias = 0.0 V

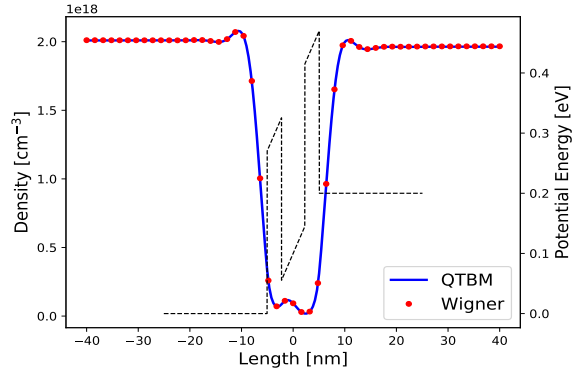

(b) Bias = 0.2 V

Fig. 3: Particle density in the active region of the RTD for different biases. The dashed black lines indicate potential energy.

References

[1] D. K. Ferry and M. Nedjalkov, *The Wigner Function in Science and Technology*. IOP Publishing, 2018.

[2] M. A. D. Gosson, *The Wigner Transform*. World Scientific, 2017.

[3] C. Zachos, D. Fairlie, and T. Curtright, *Quantum Mechanics in Phase Space*. World Scientific, 2005.

[4] J. Weinbub and D. K. Ferry, "Recent advances in Wigner function approaches," *Applied Physics Reviews*, vol. 5, no. 4, p. 041 104, 2018.

[5] A. Arnold, H. Lange, and P. F. Zweifel, "A discrete-velocity, stationary Wigner equation," *Journal of Mathematical Physics*, vol. 41, no. 11, pp. 7167–7180, 2000.

[6] R. Li, T. Lu, and Z. Sun, "Parity-decomposition and moment analysis for stationary Wigner equation with inflow boundary conditions," *Frontiers of Mathematics in China*, vol. 12, no. 4, pp. 907–919, 2017.

[7] D. Querlioz, P. Dollfus, and M. Mouis, Eds., *The Wigner Monte Carlo Method for Nanoelectronic Devices*. Wiley, 2013.

[8] R. Kosik, J. Cervenka, M. Thesberg, and H. Kosina, "A revised Wigner function approach for stationary quantum transport," in *Large-Scale Scientific Computing*, Springer International Publishing, 2020, pp. 403–410.

[9] L. Schulz and D. Schulz, "Complex absorbing potential formalism accounting for open boundary conditions within the Wigner transport equation," *IEEE Transactions on Nanotechnology*, vol. 18, pp. 830–838, 2019.